THEORETICAL MODELING OF LIDAR RETURN PHENOMENOLOGY FROM SNOW AND ICE SURFACES

J. Kerekes, J. Zhang, A. Goodenough, S. Brown

Digital Imaging and Remote Sensing Laboratory
Chester F. Carlson Center for Imaging Science, Rochester Institute of Technology,
Rochester, New York USA

ABSTRACT

To advance the science of lidar sensing of complex ice and snow surfaces as well as in support of the upcoming ICESat-2 mission, this paper establishes a framework to theoretically study a spaceborne micropulselidar returns from snow and ice surfaces. First, the anticipated lidar return characteristics for a sloped non-penetrating surface is studied when measured by a multiple-channel photon-counting detector. Second, an analytical snow reflectance model based on experimental observations is applied in synthetic scene. Based on the simulation results, the spaceborne photon-counting lidar system considered here is seen to have moderate detectability on snow surfaces. In addition, for the penetrating snow model considered here, it is shown that slightly sloped snow terrain with larger snow grain size will result in smaller elevation bias.

Index Terms— Photon counting, lidar, snow, ice

1. INTRODUCTION

Lidar sensors have been shown to be valuable sources of data to map the surface elevation and volume of glaciers [1]. A long term study is then required to monitor the amount of ice sheet balance and sea level change [2]. To serve that purpose, the Ice, Cloud and land Elevation Satellite (ICESat) was launched by NASA in 2003. Since then, by providing data on a global scale, ICESat has made great contributions on understanding ice sheets [3]. The successor of ICESat, the Ice, Cloud and land Elevation Satellite-2 (ICESat-2) is currently scheduled for launch in 2016. ICESat-2 is designed to provide elevation data to determine the temporal and spatial change of ice sheet elevation. It is also intended to measure land topography and vegetation characteristics [4]. These objectives will be achieved through the use of the Advanced Topographic Laser Altimeter System (ATLAS) on board ICESat-2, which employs 532 nm micropulse photon-counting detection.

In remote sensing, laser ranging devices actively emit pulses of short duration in visible or infrared domain of the spectrum. Compared to conventional waveform lidar sensing, it has been theoretically demonstrated that spaceborne lidar performance can be enhanced when operating in a photon-counting mode, by emitting laser pulses in a high frequency ($\sim$ kHz) train and employing single photon detection [5]. Previous work has addressed the impact of clouds on surface altimetry from spaceborne photon-counting lidars [6]. In support of future lidar sensing satellite missions, such as the upcoming ICESat-2 [4], a joint research project is ongoing between the Rochester Institute of Technology (RIT) and the University at Buffalo to study lidar sensing of snow and ice surfaces. This paper reports on some of the progress since the presentation of initial work at IGARSS 2012 [7].

2. PHOTON-COUNTING LIDAR MODELING

In this section, details on spaceborne photon-counting lidar modeling will be discussed below, including laser transmitter and multiple channel PMT.

2.1. Transmitter

ICESat-2's laser transmitter source is a 10 kHz pulse rate microchip that emits 532 nm micropulse beams. These beams are grouped into 3 sets of twins yield six footprints in total, with 45 m spacing between twin beams and 3 km spacing between sets. As can be seen in Fig. 1, for each laser firing, each photon packet emitted by the laser transmitter is spatially modeled as circular Gaussian with a 10 m diameter on the ground. In addition, the temporal shape of laser photons is also modeled with Gaussian distribution, with a 1 ns FWHM (Full Width Half Maximum) pulse width. Laser along-track sampling is 0.7 m based on the latest design of ICESat-2. For the reason of simplicity, the simulation only considers one laser beam and the underlying terrain it reaches, rather than the six beams that will be the case for ICESat-2.

2.2. Receiver

2.2.1. Number of arriving photons

As a stochastic process, the number of photons arriving at the detector can be modeled with Poisson distribution:

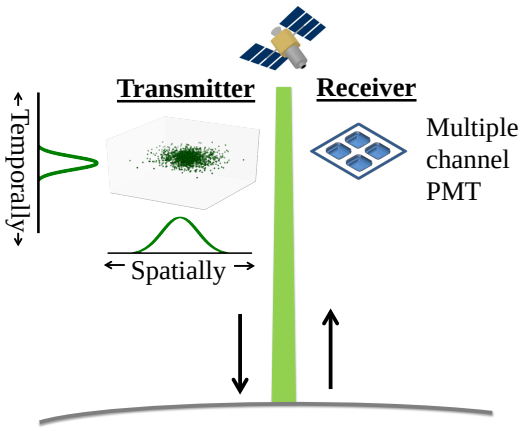

Fig. 1. Illustration of photon-counting lidar modeling.

$$p_k(\lambda) = \frac{\lambda^k}{k!} e^{-\lambda} \tag{1}$$

where $p_k(\lambda)$ is the probability to have k arriving photons when the average number is λ. Based on the current design of ICESat-2 system, it requires a probability of 80% for photons returning in clear sky for typical surfaces [4]. Therefore, the probability of no photon return ($p_0(\lambda)$) is used below to derive probability of more than one photon return:

$$p_{>0}(\lambda) = 1 - p_0(\lambda) = 1 - e^{-\lambda} \tag{2}$$

To achieve $p_k(\lambda) > 80\%$, $\lambda = 2$ is a good approximation (for $\lambda = 2$, $p_k(\lambda) = 0.86$).

In addition, photon detection efficiency (PDE) is assumed to be 50%, which represents the triggering probability for arriving photons. Note that λ will need to increase to 4 due to PDE modeling, since more photons are required to trigger the detector.

2.2.2. Multiple channel PMT

The current design for the receiver on board ICESat-2 is a PMT with single photon detectability. However, due to detector dead time, once triggered it will not register any additional arriving photons until after a period of time, typically 3 ns. Thus, the derived surface elevation will be biased toward the photon which arrives early, and this will make the surface appear higher than reality [6]. This effect is called first photon bias. To mitigate the bias created by dead time, multiple channels are utilized in the PMT.

To simulate a multiple channel design, the PMT is modeled to have segmented anodes, which can create outputs separately (as demonstrated in Fig. 1). For most of the rest of this paper, a 2×2 segmented PMT design is utilized, and each channel can be triggered independently with a 3 ns dead time. Compared to a single channel detector, multiple channel designs quantitatively improve detection accuracy on elevation retrieval, as will be demonstrated in detail in the Results and Discussion section.

For a satellite mission, noise such as solar background photons and detector dark current will also be recorded by the receiver. For simplicity, a clear sky is considered in our simulation.In other words, the simulation below assumes a algorithm will be applied in data analysis that separates ground returns from noise returns.

2.3. Elevation retrieval statistics

To evaluate the performance of spaceborne lidar systems, we define "reference elevation" as the mean value of a circle area within the laser beamwidth for each laser shot. The accuracy of the ICESat-2 derived elevation is determined by comparing the retrieved elevation with the reference elevation. Statistically, the mean and standard deviation for differences between the retrieved and reference elevation will be computed. Hereafter, we refer to the mean difference as "elevation bias."

3. MODELING OF SNOW SURFACE

Modeling of the radiometry using synthetic surfaces requires assignment of reflective properties of the surface materials. Here a model presented by Kokhanovsky and Breon [8] in a slightly modified notation is utilized in our paper:

$$\begin{aligned} R(\mu_s, \mu_v, \varphi) =& R_0(\mu_s, \mu_v, \varphi) \\ & \times \exp[-\alpha K_0(\mu_s) K_0(\mu_v) / R_0(\mu_s, \mu_v, \varphi)] \end{aligned} \tag{3}$$

$$R_0(\mu_s, \mu_v, \varphi) = \frac{a + b(\mu_s + \mu_v) + c\mu_s\mu_v + p(\theta)}{4(\mu_s + \mu_v)} \tag{4}$$

$$K_0(\mu_s, \mu_v, \varphi) = \frac{3}{7}(1 + 2\mu) \tag{5}$$

$$p(\theta) = 11.1 \exp(-0.087\theta) + 1.1 \exp(-0.014\theta) \tag{6}$$

$$\begin{aligned} \cos(\theta) &= -\mu_s\mu_v + s_s s_v \cos(\varphi) \;\; \mu_s = \cos(\vartheta_s) \\ \mu_v &= \cos(\vartheta_v) \;\; s_s = \sin(\vartheta_s) \;\; s_v = \sin(\vartheta_v) \end{aligned} \tag{7}$$

where $\alpha = \sqrt{\gamma L}$ and $\gamma = 4\pi(\chi + M)/\lambda$, χ is the imaginary part of ice refractive index, λ is the wavelength, and ϑ_s and ϑ_v represent incidence and viewing zenith angle, while φ is the relative azimuth angle (RAA). The value of L is approximately equal to $13d$, where d is the average optical diameter of snow grains.

In our simulation, laser wavelength is set as 532 nm with χ=2.54×10^{-9}, respectively. In addition, parameter M is set to be 5.5×10^{-8}, with a = 1.247, b = 1.186, c = 5.157, based on Kokhanovsky's paper [8]. Therefore, reflectance distribution can be derived using this model given a specific snow grain size d.

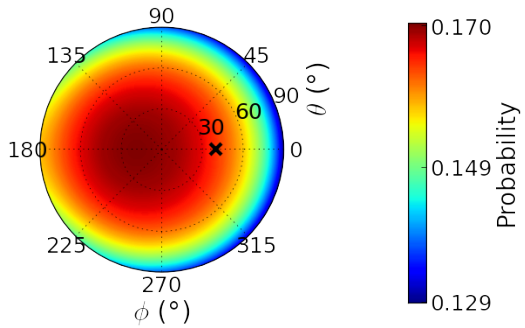

(b) θ_s=40°

Fig. 2. Reflection probability distribution for snow BRDF model with $d = 200\ \mu m$ and incident angle $\theta_s = 40°$ and $\phi_s = 0°$, denoted by black cross in figure.

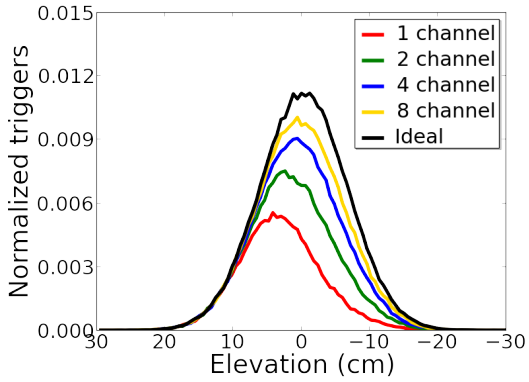

Fig. 3. Number of normalized triggers versus flat surface elevation retrievals for different numbers of PMT channels.

For a spaceborne lidar system, returning photons only in the backscattering direction will be collected by the detector. Hence, given a light incident angle, reflection probability in the backscattering direction can be calculated to derive the number of average returning photons. A example plot for reflection probability distribution is shown in Fig. 2, with incident angle $\theta_s = 40°$ and $\phi_s = 0°$. Therefore, by comparing the snow surface backscattering probability with that of a Lambertian surface, average returning photons for flat and sloped snow surface can be achieved.

4. RESULTS AND DISCUSSION

Having completed the framework for system modeling, simulation for spaceborne photon-counting lidars can now be obtained.

4.1. Flat surfaces

To demonstrate the improvement on elevation retrieval using a multiple channel PMT, $N = 100,000$ laser shots are simulated on flat surfaces. For each individual laser shot, the number of arriving photons will follow a Poisson distribution with $\lambda = 4$. Snow grain size is set to be 200 μm. Fig. 3 shows the histogram of surface elevation derived from arriving photons, with different colors representing different numbers of channels in the detector.

Since all photon events can be registered by an ideal detector, the retrieved elevation for the ideal case shows no bias. For a realistic detector, the surface elevation results are biased toward the lidar system. As a result, the derived surface elevation is higher than the actual one. However, as the colored lines in Fig. 3 demonstrate, the averaged elevation bias can be closer to 0 when more channels are utilized in the detector. Therefore, the derived surface elevation will be more accurate using multiple channel PMT receivers.

4.2. Sloped surfaces

For sloped surfaces, the incident light angle increases as the slope angle goes up. Thus, the probability for photons being reflected in the back scattering direction varies for different slopes. The aforementioned snow BRDF suggests that fewer photons will arrive at the detector as slopes become steeper.

A detailed plot of retrieved elevation versus surface slope angle is shown in Fig. 4. The mean and standard deviation are computed using $N = 100,000$ laser shots on a sloped surface, with the slope angle ranging from 0° to 10°. Since slopes raise elevation uncertainty within a sampled area, the standard deviation for returning photons increases as the slope angle goes up for these photon-counting detectors. Hence, compared to flat surfaces, uncertainty in elevation retrieval for slopes appears to result from a combined effect of laser pulse width and surface BRDF variation. As shown in Fig. 4, the mean elevation bias for arriving photons increases from around 1 cm to 3 cm, reaching its maximum for slopes around 7°, and then decreases. Meanwhile, the standard deviation keeps going up as slope angle increases.

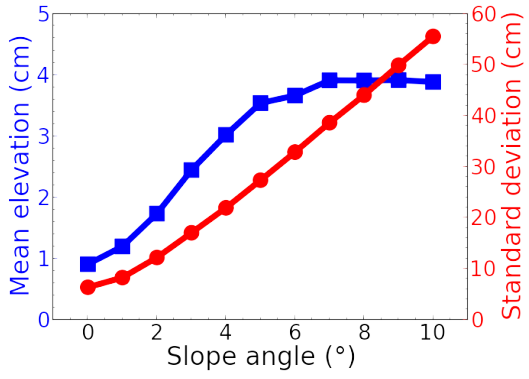

Fig. 4. Elevation retrieval of mean elevation (blue) and standard deviation (red) versus slope angle. Note the reference elevation in the case is 0 cm.

4.3. Surfaces with snow of different grain sizes

It is interesting to explore the impact of snow grain size on elevation retrieval using our framework. As discussed before, parameter L would affect the number of reflected photons in backscattering direction. In the visible region, it suggests that snow with larger grain size shows smaller reflectance. However, it is not quantitatively clear whether it will affect the elevation retrievals using spaceborne photon-counting lidar. A detailed plot of retrieved elevation versus surface slope angle in terms of different snow grain sizes is shown below in Fig. 5.

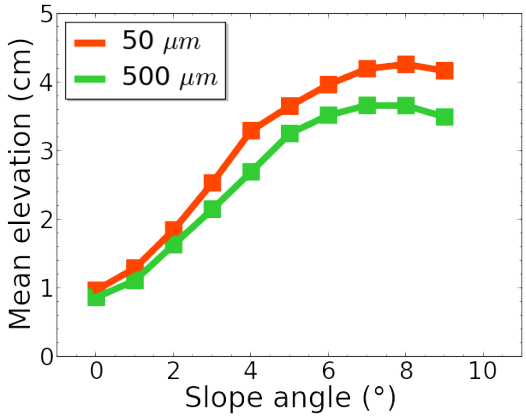

Fig. 5. Elevation retrieval of mean elevation versus slope angle for different snow grains sizes.

It is demonstrated that for slightly sloped snow surfaces, larger snow grain sizes will result in smaller elevation bias. This is due to the decrease of reflectance for snow with larger grain sizes, which is probably due to light absorption effects. This result provides a possible way to compare snow grain size by lidar measurements.

5. CONCLUSION

This paper presents some early results in quantifying the detection of lidar returns from snow and ice surfaces. A framework for the simulation of ICESat-2-like spaceborne photon-counting detector performance was presented as well as snow BRDF modeling. Even without considering atmospheric and background noise, simulation on a ICESat-2-like lidar system shows the improvement on elevation retrieval accuracy using a multiple channel design. Research is continuing to extend these results to more complex surfaces with the overall objective of contributing to the theoretical understanding of lidar sensing of complex surfaces which is anticipated to aid the analysis of data collected by future lidar systems.

6. ACKNOWLEDGEMENT

This project is supported by NASA under award number NNX11AK77G.

7. REFERENCES

[1] W. Abdalati, W. Krabill, E. Frederick, S. Manizade, C. Martin, J. Sonntag, R. Swift, R. Thomas, J. Yungel, and R. Koerner, "Elevation changes of ice caps in the canadian arctic archipelago," *Journal of Geophysical Research*, vol. 109, F04007, 2004.

[2] R.B. Alley, P.U. Clark, P. Huybrechts, and I. Joughin, "Ice-sheet and sea-level changes," *Science*, vol. 310, no. 5747, pp. 456–460, October 2005.

[3] D.C. Slobbe, R.C. Lindenbergh, and P. Ditmar, "Estimation of volume change rates of greenlands ice sheet from icesat data using overlapping footprints," *Remote Sens. Environ.*, vol. 112, no. 12, pp. 4204–4213, December 2008.

[4] W. Abdalati, H.J. Zwally, R. Bindschadler, B. Csatho, S.L. Farrell, H.A. Fricker, D. Harding, R. Kwok, M. Lefsky, T. Markus, A. Marshak, T. Neumann, S. Palm, B. Schutz, B. Smith, J. Spinhirne, and C. Webb, "The icesat-2 laser altimetry mission," *Proc. of IEEE*, vol. 98, no. 5, pp. 735–751, May 2010.

[5] J.J. Degnan, "Photon-counting multikilohertz microlaser altimeters for airborne and spaceborne topographic measurements," *J. Geodyn.*, vol. 34, no. 3-4, pp. 503–549, 2002.

[6] Y. Yang, A. Marshak, S. Palm, T. Varnai, and W. Wiscombe, "Cloud impact on surface altimetry from a spaceborne 532 nm micro-pulse photon counting lidar: system modeling for cloudy and clear atmospheres," *IEEE Trans. Geosci. Remote Sens.*, vol. 49, no. 12, pp. 4910–4919, December 2011.

[7] J. Kerekes, A. Goodenough, S. Brown, J. Zhang, B. Csatho, A. Schenk, S. Nagarajan, and R. Wheelwright, "First principles modeling for lidar sensing of complex surface," in *Proc. 2012 IEEE International Geoscience and Remote Sensing Symposium (IGARSS)*, Munich, Germany, 2012, pp. 3241–3244.

[8] A.A. Kokhanovsky and F. M. Bréon, "Validation of an analytical snow brdf model using parasol multi-angular and multispectral observations," *IEEE Geoscience and Remote Sensing Letters*, vol. 9, pp. 958–932, September 2012.